PHYSICAL REVIEW D **85,** 024045 (2012)

Stable phases of boson stars

Burkhard Kleihaus, Jutta Kunz, and Stefanie Schneider
Institut für Physik, Universität Oldenburg, D-26111 Oldenburg, Germany
(Received 28 September 2011; published 26 January 2012)

We analyze the physical properties of boson stars, which possess counterparts in flat space-time, Q-balls. Applying a stability analysis via catastrophe theory, we show that the families of rotating and nonrotating boson stars exhibit two stable regions, separated by an unstable region. Analogous to the case of white dwarfs and neutron stars, these two regions correspond to compact stars of lower and higher densities. Moreover, the high density phase ends when the black hole limit is approached. Here another unstable phase is encountered, exhibiting the typical spiralling phenomenon close to the black hole limit. When the interaction terms in the scalar field potential become negligible, the properties of mini-boson stars are recovered, which possess only a single stable phase.

DOI: 10.1103/PhysRevD.85.024045 PACS numbers: 04.20.Jb, 04.25.D−, 04.40.−b, 04.40.Dg

I. INTRODUCTION

After stars have consumed their nuclear fuel, they end their lives as compact astrophysical objects, and turn into white dwarfs, neutron stars (or their variants), or black holes, depending on their initial mass. When one investigates the equilibrium properties of compact stellar configurations, as discussed, for instance, by Shapiro and Teukolsky [1], one finds two stable phases for such compact stellar objects. These stable phases correspond to the white dwarf phase and the neutron star phase, where equilibrium is achieved by the electron and the neutron degeneracy pressure, respectively. The two stable phases are separated by an intermediate unstable phase. Moreover, the stable neutron star phase is followed by an unstable phase, exhibiting a spiralling behavior (when the mass is considered as a function of the radius). As seen in Fig. 1, the stable neutron star phase ends and the unstable phase sets in, when the black hole limit is approached.

Representing hypothetical astrophysical objects, boson stars have received considerable attention since being proposed by Feinblum and McKinley [2], Kaup [3], and Bonazzola and Ruffini [4]. Boson stars are obtained when a massive complex scalar field is coupled to gravity. The conserved Noether current associated with the global U(1) symmetry is related to their particle number Q. The physical properties of boson stars depend crucially on the rest mass of the bosons and on the presence and type of self-interaction of the bosons (see e.g. the review articles [5–9]).

When only a mass term is present but no self-interaction of the scalar field, the resulting family of mini-boson stars possesses one stable branch of solutions, which ends at the maximal mass configuration and is followed by an unstable set of solutions with spiralling behavior. The maximal mass $M_{\rm max}$ is on the order of the Planck mass squared, divided by the boson mass: $M_{\rm Pl}^2/m_{\rm B}$. When a repulsive quartic self-interaction is included, the resulting family of boson stars retains a single stable branch, but the maximal mass $M_{\rm max}$ is now on the order of $\sqrt{\lambda}M_{\rm Pl}^3/m_{\rm B}^2$, where λ is the self-coupling constant [10]. Thus, as shown by Colpi, Shapiro, and Wasserman [10], boson stars with much larger masses are obtained.

Friedberg, Lee, and Pang [11] considered boson stars with a self-interaction of the scalar field that allows for nontopological soliton solutions, also called Q-balls, even in the absence of gravity. They estimated that the maximal mass of such boson stars is on the order of $M_{\rm Pl}^4/m_{\rm B}^3$ [5].

Boson stars are obtained as stationary solutions of the coupled Einstein-scalar field equations, when the scalar field has a harmonic time dependence. The associated frequency ω_s is bounded from above by the scalar mass $m_{\rm B}$, while its lower bound depends on the details of the model. Boson stars may rotate [12–18]. Since their total angular momentum is quantized in terms of their particle number, $J = nQ$, boson stars may change their angular momentum only in discrete steps [12].

Also, boson stars with two complex scalar fields have been considered, leading to interesting phenomena due to their interaction [19–21]. The influence of a negative cosmological constant has been investigated in [22].

The stability of boson stars has been addressed from various points of view. Whereas Lee and Pang [23] performed a linear stability analysis of boson stars with respect to small oscillations, Kusmartsev, Mielke, and Schunck [24,25] applied catastrophe theory to extract the stable branches of families of boson stars. Catastrophe theory has been introduced by Thom in the 1960s [26], with further developments made by Zeeman [27], Poston and Stewart [28,29], Arnol'd [30,31], and many others. Applications to solitons have been discussed by Kusmartsev [32].

Here we analyze the properties and, in particular, the stability of boson stars obtained with quartic and sextic self-interaction terms, as introduced by Friedberg, Lee, and Pang in their nontopological soliton model [11,33]. Indeed, the existence of a flat space-time limit is of profound importance for the properties of these boson stars, as we

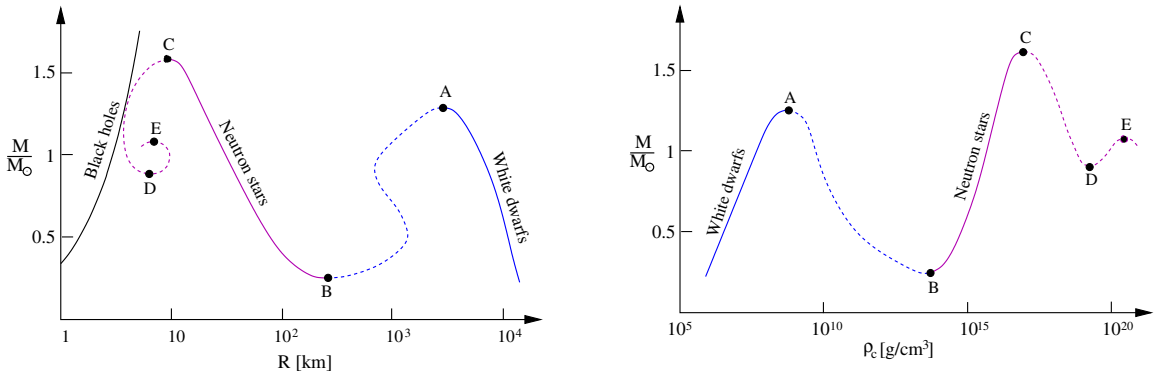

FIG. 1 (color online). Schematic diagram of the mass versus the radius (left panel) and the mass versus the central density (right panel) of compact stars, following Shapiro and Teukolsky [1].

will show below. With respect to stability we adapt the procedure of Tamaki and Sakai [34,35]. They analyzed the stability of spherically symmetric Q-balls and boson stars via catastrophe theory under primarily mathematical points of view. Here we extend this analysis to rotating boson stars.

In Sec. II we present the action, the equations of motion, and the definition of the global charges for nonrotating and rotating boson stars. In Sec. III we analyze the physical properties of the families of boson stars, presenting first the results for the nonrotating case and then for the rotating case. We give our conclusions in Sec. IV. The Appendix addresses briefly the construction of the solutions.

II. MODEL

A. Action

We consider the action of a self-interacting complex scalar field Φ coupled to Einstein gravity,

$$S = \int\left[\frac{R}{16\pi G} - \frac{1}{2}g^{\mu\nu}(\Phi^*_{,\mu}\Phi_{,\nu} + \Phi^*_{,\nu}\Phi_{,\mu}) - U(|\Phi|)\right] \times \sqrt{-g}d^4x, \tag{1}$$

where R is the curvature scalar, G is Newton's constant, the asterisk denotes complex conjugation,

$$\Phi_{,\mu} = \frac{\partial\Phi}{\partial x^\mu}, \tag{2}$$

and U denotes the potential

$$\begin{aligned} U(|\Phi|) &= \lambda|\Phi|^2(|\Phi|^4 - a|\Phi|^2 + b) \\ &= \lambda(\phi^6 - a\phi^4 + b\phi^2), \end{aligned} \tag{3}$$

with $|\Phi| = \phi$. The potential is chosen such that nontopological soliton solutions [11], also referred to as Q-balls, exist in the absence of gravity. The potential has a minimum at $\Phi = 0$, $U(0) = 0$, and a second minimum at some finite value of $|\Phi|$. The boson mass is given by $m_B = \sqrt{\lambda b}$.

Variation of the action with respect to the metric leads to the Einstein equations

$$G_{\mu\nu} = R_{\mu\nu} - \tfrac{1}{2}g_{\mu\nu}R = \bar{\kappa}T_{\mu\nu}, \tag{4}$$

with $\bar{\kappa} = 8\pi G$ and stress-energy tensor $T_{\mu\nu}$,

$$T_{\mu\nu} = g_{\mu\nu}L_M - 2\frac{\partial L}{\partial g^{\mu\nu}} \tag{5}$$

$$= -g_{\mu\nu}\left[\frac{1}{2}g^{\alpha\beta}(\Phi^*_{,\alpha}\Phi_{,\beta} + \Phi^*_{,\beta}\Phi_{,\alpha}) + U(\phi)\right] + (\Phi^*_{,\mu}\Phi_{,\nu} + \Phi^*_{,\nu}\Phi_{,\mu}). \tag{6}$$

Variation with respect to the scalar field leads to the matter field equation,

$$\left(\Box + \frac{\partial U}{\partial|\Phi|^2}\right)\Phi = 0, \tag{7}$$

where $\Box$ represents the covariant d'Alembertian operator. Equations (4) and (7) represent the set of coupled Einstein-Klein-Gordon equations.

B. Ansatz

To obtain stationary axially symmetric solutions, we impose on the space-time the presence of two commuting Killing vector fields, ξ and η, where

$$\xi = \partial_t, \qquad \eta = \partial_\varphi \tag{8}$$

in a system of adapted coordinates $\{t, r, \theta, \varphi\}$. In these coordinates the metric is independent of t and φ, and can be expressed in isotropic coordinates in the Lewis-Papapetrou form [36–39]

$$ds^2 = -fdt^2 + \frac{l}{f}\left[h(dr^2 + r^2d\theta^2) + r^2\sin^2\theta\left(d\varphi - \frac{\omega}{r}dt\right)^2\right]. \tag{9}$$

The four metric functions f, l, h, and ω are functions of the variables r and θ only.

The symmetry axis of the space-time, where $\eta = 0$, corresponds to the z axis. The elementary flatness condition

$$\frac{X_{,\mu}\, X^{,\mu}}{4X} = 1, \qquad X = \eta^{\mu}\eta_{\mu} \tag{10}$$

then imposes on the symmetry axis the condition [36]

$$h|_{\theta=0} = h|_{\theta=\pi} = 1. \tag{11}$$

For the scalar field Φ we adopt the stationary ansatz [12]

$$\Phi(t, r, \theta, \varphi) = \phi(r, \theta)e^{i\omega_s t + in\varphi}, \tag{12}$$

where $\phi(r, \theta)$ is a real function, and ω_s and n are real constants. Single-valuedness of the scalar field requires

$$\Phi(\varphi) = \Phi(2\pi + \varphi); \tag{13}$$

thus the constant n must be an integer, i.e., $n = 0, \pm 1, \pm 2, \ldots$. We refer to n as the rotational quantum number, since for $n \neq 0$ axially symmetric rotating boson stars arise, whereas for $n = 0$ spherically symmetric nonrotating boson stars are obtained.

Solutions with positive and negative parity satisfy, respectively,

$$\phi(r, \pi - \theta) = \phi(r, \theta), \tag{14}$$

$$\phi(r, \pi - \theta) = -\phi(r, \theta). \tag{15}$$

C. Global charges

The mass M and the angular momentum J of stationary asymptotically flat space-times can be obtained from their respective Komar expressions [40],

$$M = \frac{1}{4\pi G}\int_{\Sigma} R_{\mu\nu}n^{\mu}\xi^{\nu}dV \tag{16}$$

and

$$J = -\frac{1}{8\pi G}\int_{\Sigma} R_{\mu\nu}n^{\mu}\eta^{\nu}dV. \tag{17}$$

Here Σ denotes an asymptotically flat spacelike hypersurface, n^{μ} is normal to Σ with $n_{\mu}n^{\mu} = -1$, dV is the natural volume element on Σ, ξ denotes an asymptotically timelike Killing vector field, and η is an asymptotically spacelike Killing vector field [40]. When the Ansatz Eq. (9) is inserted into the Komar expressions Eqs. (16) and (17), the integrals simplify, yielding the mass M and the angular momentum J directly in terms of the asymptotic behavior of the metric functions f and ω, respectively [38],

$$M = \frac{1}{2G}\lim_{r\to\infty} r^2\partial_r f, \qquad J = \frac{1}{2G}\lim_{r\to\infty} r^2\omega. \tag{18}$$

A conserved charge Q is associated with the complex scalar field Φ, since the Lagrange density is invariant under the global phase transformation

$$\Phi \longrightarrow \Phi e^{i\alpha} \tag{19}$$

leading to the conserved current

$$j^{\mu} = -i(\Phi^*\partial^{\mu}\Phi - \Phi\partial^{\mu}\Phi^*), \qquad j^{\mu}{}_{;\mu} = 0. \tag{20}$$

The conserved scalar charge Q is obtained from the time-component of the current,

$$\begin{aligned} Q &= -\int j^t |g|^{1/2} dr d\theta d\varphi \\ &= 4\pi\omega_s \int_0^{\infty}\int_0^{\pi} |g|^{1/2}\frac{1}{f}\left(1 + \frac{n}{\omega_s}\frac{\omega}{r}\right)\phi^2 dr d\theta. \end{aligned} \tag{21}$$

As first derived by Schunck and Mielke [12], one obtains a quantization relation for the angular momentum in terms of the charge,

$$J = nQ. \tag{22}$$

Thus a spherically symmetric boson star has angular momentum $J = 0$, because $n = 0$.

D. Units

We choose for the potential $U(\phi)$, Eq. (3), the following set of fixed parameters [17,18,33]:

$$\lambda = 1, \qquad a = 2, \qquad b = 1.1 = \mu_0^2. \tag{23}$$

The equations then depend only on the dimensionless coupling constant κ,

$$\kappa = 8\pi G\left(\frac{m_{\mathrm{B}}}{\mu_0^2}\right)^2. \tag{24}$$

Since κ consists of a product of Newton's constant and the square of the boson mass, we may interpret a change of its numerical value in two ways: either as a change of the gravitational coupling for a fixed boson mass, or as a change of the boson mass for a fixed value of the gravitational coupling.

To obtain the respective dimensionful values of the physical properties, M^{phys}, Q^{phys}, J^{phys}, we have to scale the numerically calculated values for the mass M^{num}, the charge Q^{num}, and the angular momentum J^{num} appropriately. Therefore we introduce the parameter q_0,

$$q_0 = \left(\frac{m_{\mathrm{Pl}}}{m_{\mathrm{B}}}\right)^2\frac{1}{8\pi}, \tag{25}$$

where m_{Pl} is the Planck mass, and find

TABLE I. Scale factors for the physical properties.

m_{B}	q_0	$q_0 m_{\mathrm{B}}$	σ
1 GeV/c^2	$\approx 10^{36}$	$\approx 10^{36}$ GeV/c^2	$\approx 0.2\mu_0$ fm
10^{-19} GeV/c^2	$\approx 4\times 10^{74}$	$\approx M_{\mathrm{sun}}$	$\approx 0.2\mu_0 10^4$ m

$$Q^{\rm phys} = \mu_0^2 \bar{\kappa} q_0 Q^{\rm num}, \qquad M^{\rm phys} = \mu_0 \bar{\kappa} q_0 m_{\rm B} M^{\rm num}, \qquad J^{\rm phys} = n\hbar Q^{\rm num}. \tag{26}$$

The length scale is set by

$$\sigma = \frac{\mu_0}{m_{\rm B}} \approx \frac{\mu_0}{m_{\rm B}[\rm GeV]} \times 0.2 \times 10^{-15}\ \rm m.$$

Two examples for the scales of the physical properties are exhibited in Table I. The first corresponds to a scalar particle with a mass on the order of the proton mass, whereas the second corresponds to a very light scalar particle, chosen such that the mass scale $q_0 m_{\rm B}$ is set by the solar mass.

III. BOSON STAR PROPERTIES

A. Spherically symmetric boson stars

1. Equilibrium space

Let us first consider the families of fundamental spherically symmetric boson stars ($n = 0$) as obtained in [17,18]. (In fundamental boson stars the scalar field is a monotonically decreasing function, whereas in radially excited boson stars, it possesses nodes.) For a fixed value of the dimensionless coupling constant κ, Eq. (24), a family of stationary solutions exists in the frequency range $\omega_0(\kappa) \leq \omega_s \leq \omega_{\rm max}$. The minimal frequency $\omega_0(\kappa)$ depends on κ and increases with κ, tending to finite limits as $\kappa \to 0$ and $\kappa \to \infty$ [17]. The maximal frequency $\omega_{\rm max}$ is always given by the boson mass.

All families of solutions together form the equilibrium space, which we denote by $\mathcal{M} = \{\omega_s, \kappa, Q\}$. To illustrate the equilibrium space we have exhibited several families of solutions in Fig. 2. For each family (with fixed κ) the frequency ω_s is shown versus the particle number Q. The coupling constant κ assumes values in the range $0.0002 \leq \kappa \leq 1$ in the figure. We thus cover the full range of distinct theoretical possibilities for the behavior of these boson star solutions [17,18]. The equilibrium space may then be pictured as the surface obtained when κ varies continuously from zero to infinity.

The families of solutions have two important features in common. They all start from particle number $Q = 0$ at the upper limit of the frequency, and they all form spirals towards their lower frequency limit. In between, however, a qualitative change of the curves is observed, as the value of κ increases. The salient maximum value of Q in the small frequency range as well as the finite (relative) minimum value of Q, which are both present for small values of the coupling constant κ, become less pronounced with increasing κ, until they merge and disappear altogether.

We may also consider the set of equilibrium solutions with respect to another set of parameters. Instead of the frequency ω_s we may consider the finite value $\phi_0 = \phi(0)$ of the scalar field at the origin. (We recall that in these fundamental boson star solutions the scalar field decreases monotonically from the origin to zero at infinity.) Moreover, instead of the particle number Q we may consider the mass M of the solutions.

We exhibit the same families of solutions as above for this choice of variables in Fig. 3. Here, for each family of solutions (with fixed κ) the value of the scalar field ϕ_0 is shown versus the mass M. We note, however, that the range of ϕ_0 has been truncated in the figure, being limited to the range $0 \leq \phi_0 \leq 2$. Inside the spiral ϕ_0 certainly assumes larger values, and indeed increases monotonically as the mass exhibits damped oscillations [17]. The equilibrium space $\mathcal{N} = \{\phi_0, M, \kappa\}$ may then again be pictured as the surface obtained when κ varies continuously from zero to infinity.

2. Binding energy and cusp structure

To get a better physical understanding of these boson stars that form the equilibrium space, let us next address their binding energy $B = m_{\rm B} Q - M$. We exhibit the binding energy B in Fig. 4 for two families of solutions,

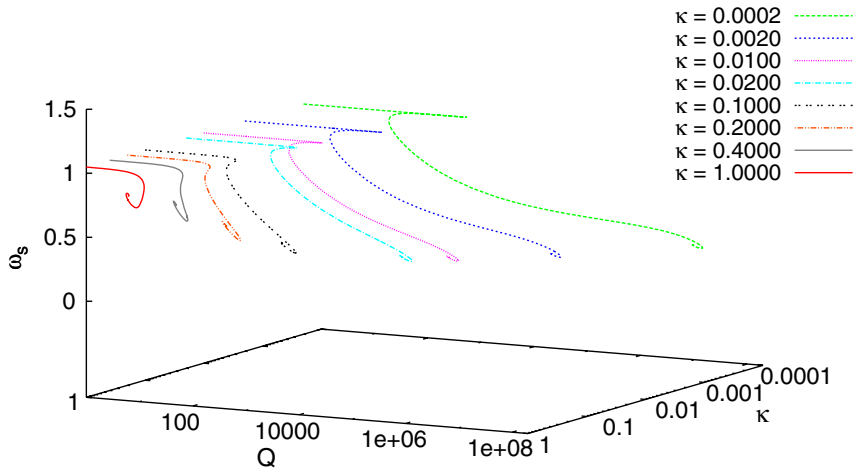

FIG. 2 (color online). Equilibrium space $\mathcal{M} = \{\omega_s, Q, \kappa\}$ for fundamental boson stars in the range $0.0002 \leq \kappa \leq 1$.

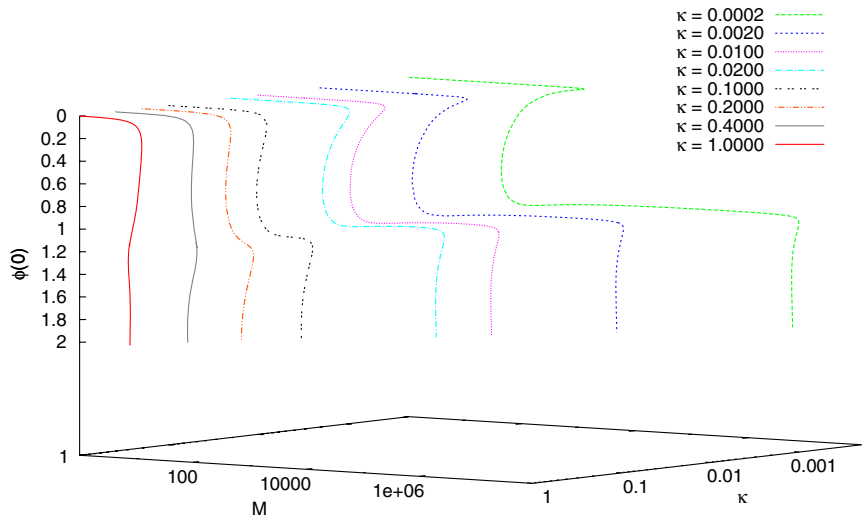

FIG. 3 (color online). Equilibrium space $\mathcal{N} = \{\phi_0, M, \kappa\}$ for fundamental boson stars in the range $0.0002 \leq \kappa \leq 1$.

corresponding to typical examples in the lower κ range, namely, $\kappa = 0.01$ and $\kappa = 0.02$. While at first glance all solutions seem to be bound, with their binding energy increasing almost linearly with their particle number, a closer look at the solutions in the high frequency range (ω_s close to m_B) reveals a bifurcation structure involving two cusps.

Clearly, a first branch of bound boson star solutions resides between the vacuum $M = Q = 0$ and a local maximum of the mass and charge, M_A, Q_A, at the first cusp A. A second branch, where the mass and charge decrease monotonically, connects the first cusp A with the second cusp B, where the mass and charge have a local minimum, M_B, Q_B. Most of this branch resides in the unbound region. The third branch emerges from the second cusp B and extends up to the third cusp C, where the mass and charge reach their global maximum, M_C, Q_C. Along this third branch the mass and charge increase monotonically. The solutions are unbound only in the vicinity of the second cusp B, since the binding energy crosses the zero already at the point u, located close by. At the third cusp C the binding energy is also maximal.

We exhibit in Fig. 5 the physical characteristics of these three cusps, A, B, and C. As $\kappa \to 0$, the values of the mass M_A and the charge Q_A at the cusp A increase, tending to infinity with the power $\kappa^{-1/2}$, as illustrated in Fig. 5 by the curves $M_{A,\mathrm{lim}}$ and $Q_{A,\mathrm{lim}}$. The values of the mass M_B and the charge Q_B at the cusp B show a very different behavior. They tend to constant values in the limit $\kappa \to 0$, corresponding to the values of the mass and the charge of the unique minimum of the Q-ball solutions of flat space-time. This is also illustrated in Fig. 5. At the cusp C the values of the mass M_C and the charge Q_C increase again without bound as $\kappa \to 0$. As extrapolated previously [17], the limiting behavior is of the form $M_C \sim \kappa^{-3/2}$, $Q_C \sim \kappa^{-3/2}$, which is also shown in the figure.

Turning to the larger values of κ, we note that the two extrema B and C, and thus the two cusps B and C, merge and disappear at a critical value κ_{cr}. Thus beyond κ_{cr}, from the three cusps A, B, and C, only the cusp A is left.

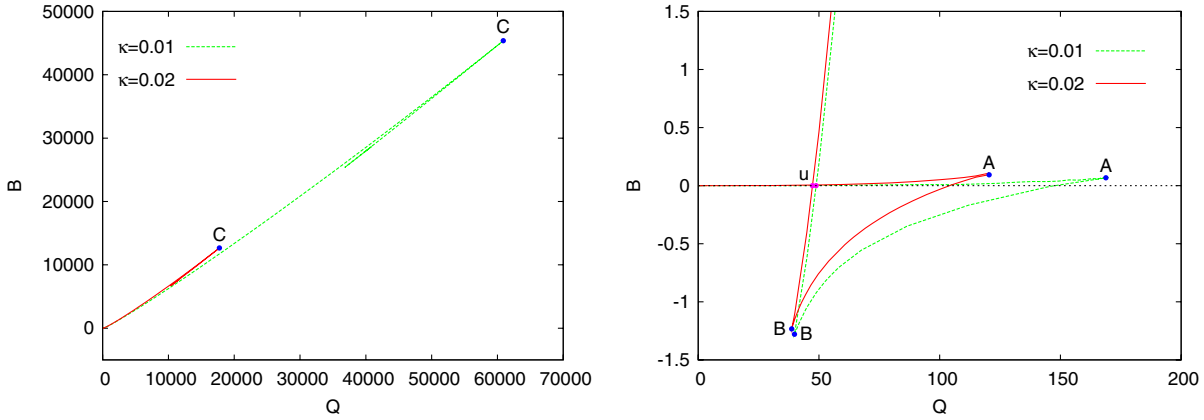

FIG. 4 (color online). Binding energy $B = M - m_{\mathrm{B}}Q$ for two families of solutions, corresponding to $\kappa = 0.01$ and $\kappa = 0.02$, respectively. The right figure zooms into the high frequency range.

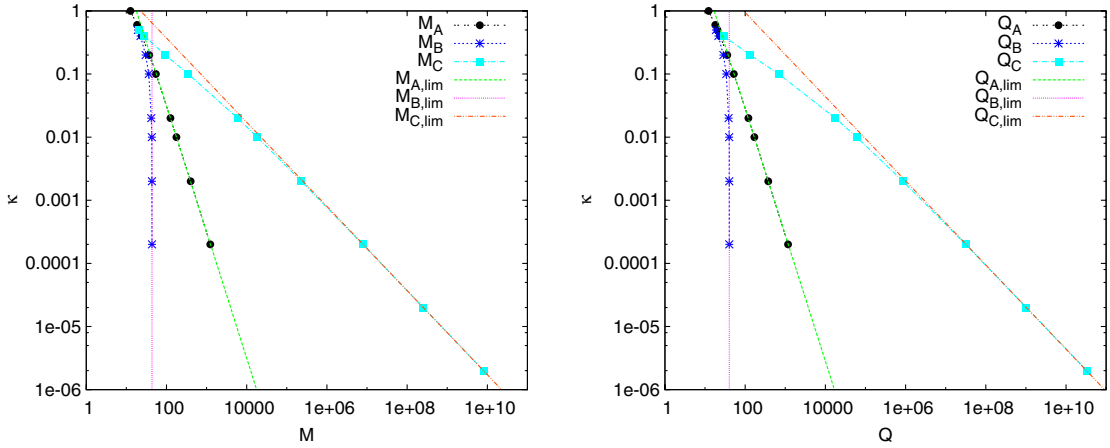

FIG. 5 (color online). Coupling constant κ versus the mass M (left panel) and versus the particle number Q (right panel) for the cusps A, B, and C, together with functions approximating their behavior in the limit $\kappa \to 0$. Note that for the larger values of κ, the cusps B and C are no longer present.

The large value of κ means, from a physical point of view, that the higher order terms in the potential become relatively less important, and the solutions tend to the well-known mini-boson star solutions. Indeed, for $\kappa \to \infty$ the mini-boson star solutions are recovered after a rescaling [17].

To complete the discussion of the branches of the families of boson star solutions, we still need to address their behavior beyond the cusp C (or for large κ, beyond the cusp A). As seen in Fig. 2 the branches form a spiral when considered in terms of the frequency ω_s and the charge Q (or the mass M). Alternatively, when considered in terms of the value of the scalar field at the origin and the mass M (or the charge Q) as in Fig. 3, a damped oscillation is seen. Thus beyond C (or for large κ, beyond A) the mass and the charge reach a minimum D, then another maximum E, another minimum F, etc., converging towards limiting values $M_{\rm lim}$, $Q_{\rm lim}$ [17]. When the mass is considered as a function of the charge, finally, this behavior translates into an intricate cusp structure [11].

3. Size and black hole limit

There is no unique definition for the radius of a boson star, and many proposals have been discussed in the literature (see e.g. [9]). Here we have chosen the definitions

$$R_1 = \frac{\int j^t |g|^{1/2} r dr}{\int j^t |g|^{1/2} dr}, \qquad R_2^2 = \frac{\int j^t |g|^{1/2} r^2 dr}{\int j^t |g|^{1/2} dr} \tag{27}$$

for the spherically symmetric boson stars, where the radial coordinate is not the isotropic coordinate introduced in Sec. II, but a Schwarzschild-like coordinate, which has an invariant circumferential meaning. Figure 6 (left panel) shows that both definitions give rather similar results for the size of the boson stars. From the radius and thus the size of the boson stars together with their mass, we obtain an estimate of their density.

Let us now discuss the relation between the mass and the size of the boson stars, focusing on the smaller values of κ (away from the mini-boson star limit). As seen in Fig. 6,

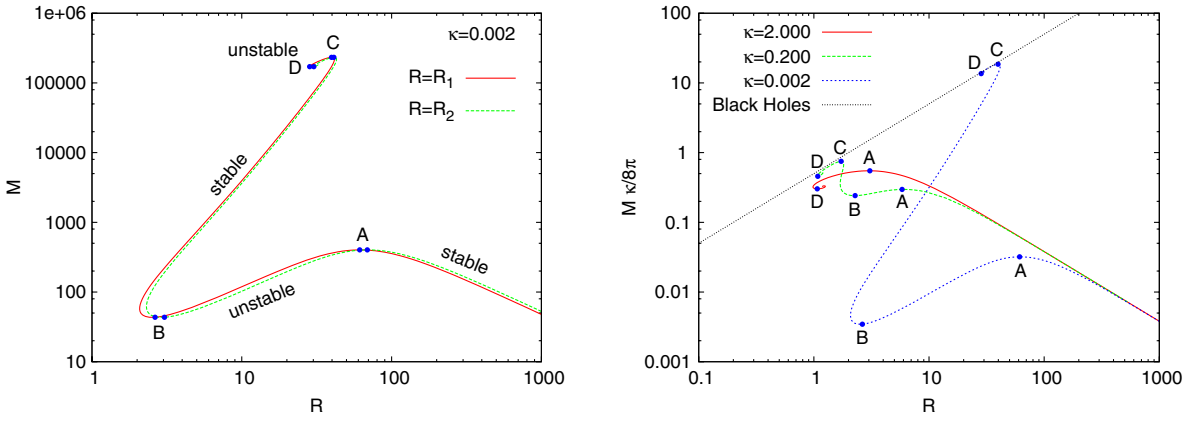

FIG. 6 (color online). A comparison of the two definitions, Eq. (27), for the boson star radius for the family of solutions with $\kappa = 0.002$ (left panel); the mass versus the boson star radius R_1 for the families of solutions with $\kappa = 2.0$, $\kappa = 0.2$, and $\kappa = 0.002$, together with the corresponding Schwarzschild black hole curve (right panel). The cusps A through D are also marked.

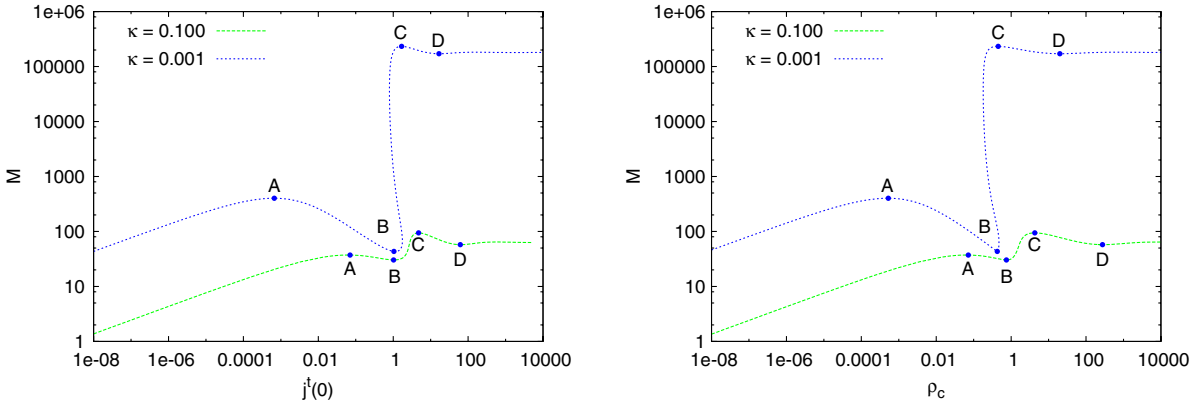

FIG. 7 (color online). The mass versus the central particle number density $j^t(0)$ (left panel) and the central energy density $\rho_c(0)$ (right panel) of the families of boson star solutions with $\kappa = 0.001$ and $\kappa = 0.1$.

the mass increases along the first branch, while the radius decreases. This is the behavior known from compact objects such as white dwarfs and neutron stars. The first branch ends at the cusp A. Beyond A the mass decreases until the second cusp B is reached, while the radius continues to decrease along this second branch. Beyond B the mass increases again, and soon rises steeply along this third branch. But the radius (soon) starts to increase as well, and then rises further along this branch, almost up to the cusp C. Such a behavior is known, in fact, for quark stars, whose radius increases with increasing mass [41,42]. Thus, while the boson stars are already compact objects on the first branch, they become even much more compact objects along the third branch.

This behavior is very reminiscent of the phases of compact fermionic stars, where the lower density stars represent white dwarfs, while the higher density stars represent neutron stars or their variants. The neutron stars cease to exist when the black hole limit is reached. Close to this limit, the solutions exhibit a spiralling behavior, as seen in the schematic drawing in Fig. 1. And indeed, when we include the black hole limit, given by the Schwarzschild relation $2GM = R$, in the figure for the boson stars, Fig. 6 (right panel), we observe that the spiral is precisely formed, when the family of boson star solutions approaches the black hole limit.

Finally, in Fig. 7 we exhibit the mass of the boson stars versus the central particle number density $j^t(0)$ (left panel) and versus the central energy density $\rho_c(0)$ (right panel). Clearly, the first branch has much lower central density than the third branch, just like the white dwarf branch and the neutron star branch of the compact fermionic stars [1].

4. Stability analysis

Let us now address the stability of these families of spherically symmetric boson stars. The above observed analogy between the branches of compact stars and the branches of boson stars suggests to begin by recalling the stability properties of the compact stars as indicated in Fig. 1, following Shapiro and Teukolsky [1].

The white dwarf branch ending at the cusp A is stable. It is followed by an unstable branch, ending at the cusp B. The neutron star branch from B to C is again a stable branch. The spiral beyond C is unstable. In particular, one mode becomes unstable at A and turns stable again at B. At C the mode becomes unstable again, and at each following extremal point in the spiral, another mode turns unstable. Thus there are two physically relevant stable branches, the lower density white dwarf branch and the higher density neutron star branch. The latter ends close to the black hole limit.

For mini-boson stars a mode analysis has been performed by Lee and Pang [23] to determine the stability of the solutions. Mini-boson stars possess only a single stable branch followed by the spiral. As in the case of the compact fermionic stars, at each following extremal point in the spiral, another mode of these boson stars turns unstable.

On the other hand, the stability of boson stars has been analyzed by invoking the arguments of catastrophe theory [24,34,35]. Some standard references to catastrophe theory can be found in [26–31]. We briefly recall the procedure employed by Tamaki and Sakai [34,35], applying it to the above family of boson star solutions.

An essential point in utilizing catastrophe theory is to select an appropriate set of behavior variable(s) and control parameter(s). A behavior variable should be a quantity that describes the behavior of the system uniquely when the control parameters change their values. Following Tamaki and Sakai [34,35], we choose the coupling constant κ and the charge Q as the two control parameters, and we choose the frequency ω_s as the single behavior variable. [In the relevant range of solutions up to the cusp C (but not beyond), the variable ω_s is indeed unique. In contrast, the variable ϕ_0 is unique in the spiral beyond the cusp C,

but is not necessarily unique in the vicinity of C right before the cusp.]

To analyze the stability of these boson stars, we start from the equilibrium space $\mathcal{M} = \{\omega_s, \kappa, Q\}$, exhibited in Fig. 2. According to catastrophe theory, the stability changes only at the turning points, where $\frac{\partial Q}{\partial \omega_s} = 0$ (for fixed values of κ). Therefore,

(i) we determine the turning points, where stability changes, denoting them by $A, B, C, \ldots$;
(ii) we plot the values of the turning points $A, B, C, \ldots$ versus κ to obtain the control space $\mathcal{C} = \{\kappa, Q\}$, to identify the regions of stability, respectively, instability.

We list the turning points in Table II together with the extrapolated values of the limiting solutions $Q_{\rm lim}$ at the centers of the spirals [17].

Each point of the equilibrium space $\mathcal{M} = \{\omega_s, \kappa, Q\}$ represents a boson star configuration. The set of turning points partitions this phase portrait into subareas. In catastrophe theory, ''stability'' means stability with respect to local perturbations. According to catastrophe theory, passing a turning point means changing the stability of the boson star configurations. The solutions between two turning points then form branches, where all the configurations possess the same kind of stability (or instability). Thus there are S and U branches representing stable and unstable configurations [43,44].

This reveals the strength of catastrophe theory: stability changes exclusively when passing a turning point, while all configurations of the considered system between two turning points possess the same kind of stability (or instability). Thus, it is sufficient to consider only a single configuration of a branch to know the stability of all the other configurations of the same branch with respect to local perturbations.

For boson star solutions we see a cusp-catastrophe because (leaving the spiral aside) their equilibrium space $\mathcal{M}$ shows the characteristics of a Whitney surface [32,45]. Therefore, we conclude that the branch from the vacuum solution to the first turning point Q_A is a stable one [32,35]. The next branch from Q_A to Q_B is unstable, and the branch from Q_B to Q_C is stable again [35]. This comprises a complete Whitney surface with stable upper and lower sheets and an unstable area in between. The next turning points are part of the spiral. Such spirals are described by Arnold [31] as ''limit cycles,'' where the equilibrium states lose their stability. Then all configurations, which are part of the spirals, are unstable. We note that this analysis is in complete agreement with the discussion above for compact fermionic stars.

The stability properties can also be illustrated schematically by the standard representation of the ''potential'' as a function of the '' behavior variable'' [32,34,35]. We exhibit in Fig. 8 (schematically) the potential function for several sets of configurations. The notation S_{X-Y} indicates a solution on the branch extending between the cusp X (respectively, vacuum 0) and the cusp Y, whereas S_X corresponds to the solution at the cusp X. Here we restrict to branches of solutions up to the cusp C, which are relevant for the discussion of the stability. The appearance of the different branches of solutions is then seen in the figure for fixed $\kappa < \kappa_{\rm cr}$ and varying Q.

For $Q < Q_B$ a single branch of stable solutions is present, corresponding to the minimum in Fig. 8(a). A saddle point appears for $Q = Q_B$ in Fig. 8(b). This saddle point splits into a maximum and a minimum in Fig. 8(c) for $Q_B < Q < Q_A$. The maximum corresponds to a solution on the unstable branch, whereas the two minima correspond to solutions on the two stable branches. The maximum and the second minimum merge to form a saddle point, when $Q = Q_A$, as shown in Fig. 8(d). Thus the branch of unstable solutions disappears for $Q > Q_A$, and a single branch of stable solutions remains in Fig. 8(e). We note that for $\kappa > \kappa_{\rm cr}$ the branch of unstable solutions between the cusps B and C is not present.

Let us finally exhibit the stability properties of the boson stars by presenting the control space $\mathcal{C} = \{\kappa, Q\}$ in Fig. 9. The control space is the projection of the catastrophe map $\chi(\mathcal{M})$ into the control plane. In the regions denoted by S_1, $S_iU(i = 1, 2)$, and N, there is one stable solution, there are i

TABLE II. Values of the charge at the turning points $A, B, C, \ldots$, and of the limiting solution $Q_{\rm lim}$ at the center of the spiral for the fundamental boson stars for several values of the coupling constant κ. As indicated by the line, the cusps B and C have merged and disappeared between $\kappa = 0.4$ and $\kappa = 1$.

κ	Q_A	Q_B	Q_C	Q_D	Q_E	Q_F	Q_{lim}
0.0002	1174.78	40.2495	3.117×10^7	2.040×10^7	2.220×10^7	2.181×10^7	2.181×10^7
0.0020	377.455	40.0820	864 746	553 687	605 046	593 437	5.954×10^5
0.0100	169.834	39.9989	60 416.2	36 845.6	40 849.6	39 949.6	4.011×10^4
0.0200	120.476	38.7401	17 702.5	10 350.7	11 593.1	11 307.0	1.136×10^4
0.1000	52.22	33.91	684.741	331.677	391.874	378.274	380.4600
0.2000	35.763	28.668	134.72	61.19	72.96	70.463	70.8330
0.4000	23.66	21.47	28.89	15.85	17.85	17.46	17.5180
1.0000	12.22	–	–	5.83	6.31	6.29	6.2114

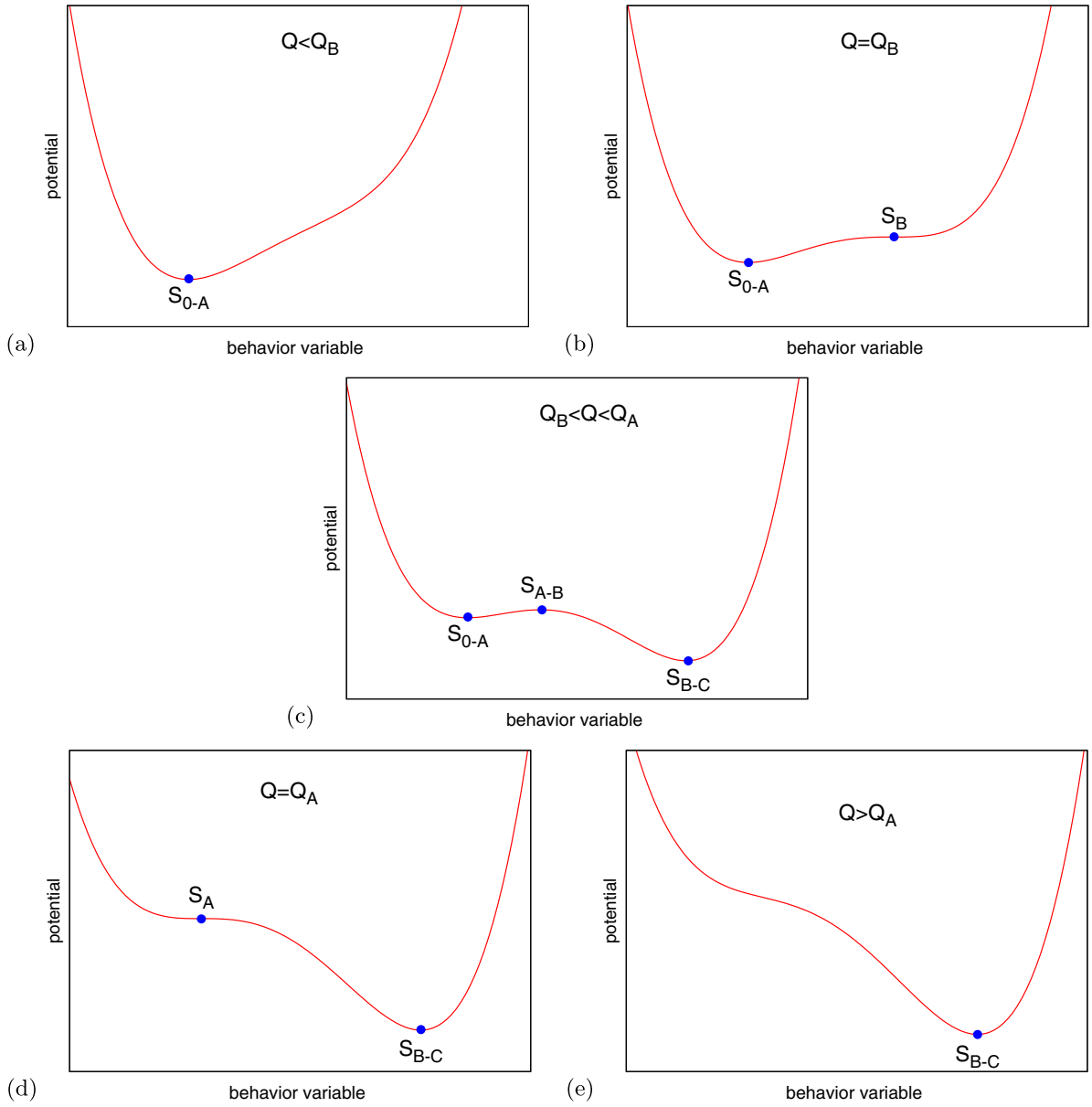

FIG. 8 (color online). Stability interpretation via the potential function for the boson stars. The boson star solutions correspond to extrema in configuration space. The appearance of the different branches of solutions is schematically demonstrated for fixed $\kappa < \kappa_{\rm cr}$ and varying Q.

stable solution(s) and one or more unstable solution(s), and there are no equilibrium solutions, respectively. The area delimited by the turning points Q_C and Q_D contains, besides one stable solution, all the unstable solutions of the spiral.

The control space reveals that there are two areas, where only a single stable solution exists. The first area is associated with the stable branch terminating at A. This is the branch formed by the stable lower density boson stars. The second area is associated with the branch from B to (almost) C. This branch comprises the stable high density boson stars. As the coupling constant κ increases, the width of the second area diminishes and shrinks to zero at the critical value of κ. This transition is consistent with the fact that for large κ the solutions tend to mini-boson star solutions, which possess only a single stable branch.

B. Rotating boson stars

Let us now turn to rotating boson stars. These stationary axially symmetric configurations have a finite angular momentum proportional to their particle number, $J = nQ$ [Eq. (22)], with the "quantum number" $n \neq 0$. In the following we extend our above analysis of the physical properties of boson stars to the rotating case, focusing on solutions with $n = 1$ and positive parity, i.e. $n = 1^+$ boson stars that were obtained previously [17,18].

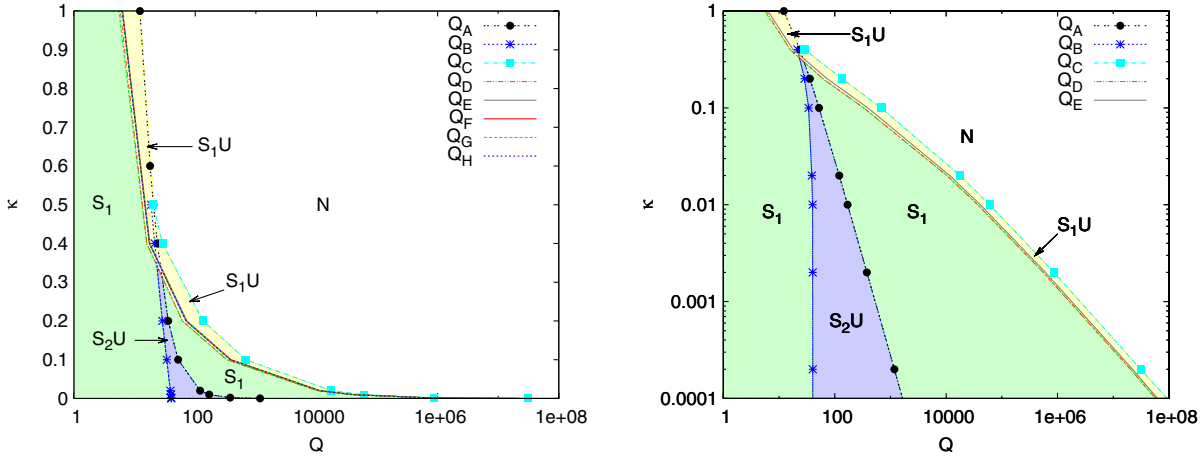

FIG. 9 (color online). Control space $\mathcal{C} = \{\kappa, Q\}$ for the fundamental boson stars. In the areas denoted by S_1, $S_iU (i = 1, 2)$, and N, there is a single stable solution, there are i stable solution(s) and one or more unstable solution(s), and there is no equilibrium solution, respectively. The axes are semilogarithmic (left panel) and double logarithmic (right panel).

1. Equilibrium space of $n = 1^+$ boson stars

As in the case of the spherically symmetric boson stars, we begin our analysis of the $n = 1^+$ rotating boson stars by considering the equilibrium space $\mathcal{M} = \{\omega_s, \kappa, Q\}$. Again, for a fixed value of the dimensionless coupling constant κ a family of stationary solutions exists in the frequency range $\omega_0(\kappa) \leq \omega_s \leq \omega_{\max}$, where $\omega_0(\kappa)$ increases with κ, whereas $\omega_{\max}$ is still given by the boson mass [17]. This is seen in Fig. 10, where we illustrate the equilibrium space $\mathcal{M} = \{\omega_s, \kappa, Q\}$ of the $n = 1^+$ boson stars.

Clearly, the structure of the equilibrium space $\mathcal{M} = \{\omega_s, \kappa, Q\}$ of the $n = 1^+$ boson stars is very similar to the one of the $n = 0$ solutions. All families of solutions (for fixed κ) start from the vacuum $Q = 0$ at the upper limit of the frequency, and all form spirals at the lower end. However, we note that as κ increases, the $n = 1^+$ spirals become more elongated in this equilibrium space with respect to ω_s than their $n = 0$ counterparts.

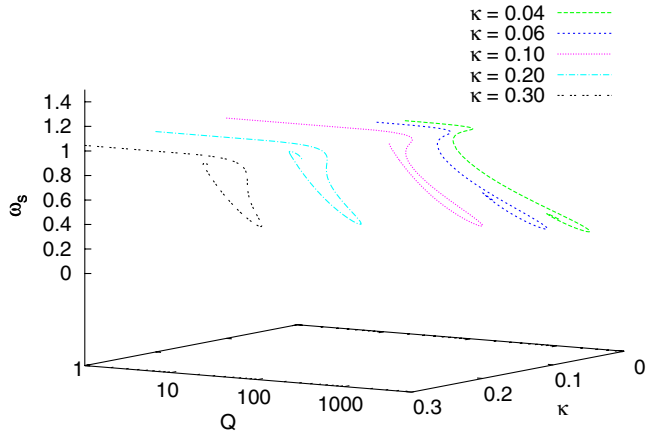

FIG. 10 (color online). Equilibrium space $\mathcal{M} = \{\omega_s, \kappa, Q\}$ for rotating boson stars with $n = 1^+$ in the range $0.04 \leq \kappa \leq 0.3$.

We could also consider the set of equilibrium solutions with respect to other sets of parameters. For the $n = 0$ boson stars we considered the alternative equilibrium space $\mathcal{N} = \{\phi_0, M, \kappa\}$. Here we would have to replace the variable ϕ_0 by another variable, however, since for rotating boson stars $\phi_0 = 0$. Such an alternative variable for $n = 1^+$ boson stars would be $\phi_0' = \phi'(0)$ [46].

2. Cusp structure of $n = 1^+$ boson stars

Let us next turn to the cusp structure of these rotating boson stars. As in the case of the $n = 0$ solutions, for not too large values of the coupling constant κ a first branch of rotating boson star solutions resides between the vacuum $M = Q = 0$ and the local maximum of the mass and charge, M_A, Q_A, at the first cusp A. Next, a second branch connects the first cusp A with the second cusp B, where the mass and charge have a local minimum, M_B, Q_B. Then a third branch emerges from the second cusp B and extends up to the third cusp C, where the mass and charge reach their global maximum, M_C, Q_C. Beyond C, finally, a spiral is formed. We list these turning points in Table III.

Analogous to the nonrotating case, the values of the mass M_A and the charge Q_A at the cusp A increase, as $\kappa \to 0$. Indeed, we observe the same $\kappa^{-1/2}$ dependence, as seen in Fig. 11. The values of the mass M_B and the charge Q_B at the cusp B, on the other hand, are expected to tend to constant values in the limit $\kappa \to 0$, corresponding now to the values of the mass and the charge of the unique minimum of the rotating Q-ball solutions in flat space-time. (The available data do not yet suffice to fully demonstrate this behavior, however.) The values of the mass M_C and the charge Q_C at the cusp C increase again without bound as $\kappa \to 0$. The available data do not yet exhibit the expected limiting $\kappa^{-3/2}$ dependence, but a somewhat deviating κ dependence. This is analogous to the nonrotating case in this range of values of the coupling constant κ, where the

TABLE III. Turning points for rotating boson stars with $n = 1^+$ for several values of the coupling constant κ.

κ	Q_A	Q_B	Q_C	Q_D
0.04	226.888	135.570	5121.20	1630.19
0.06	184.8	130.123	2408.91	434.076
0.10	140.631	118.113	910.699	77.434
0.20	96.197	94.1	237.173	35.984
0.30	–	–	110.958	23.462

limiting $\kappa^{-3/2}$ dependence is only approached for considerably smaller values of κ.

For larger values of κ, however, we observe a somewhat different pattern for the cusps A, B, and C in the case of the rotating boson stars as compared to the nonrotating case. In the rotating case, the extrema A and B merge, and disappear at a critical value of κ while C remains, as seen in Table III and Fig. 11. In the nonrotating case it is B and C which merge while A remains. In both cases, however, for large values of κ the solutions exhibit the same pattern as the mini-boson stars: they possess a single physically relevant branch, beyond which a spiral is formed.

3. Size of $n = 1^+$ boson stars

As in the case of the $n = 0$ boson stars, we would like to study the compactness of the rotating boson stars and their proximity to the black hole limit. For that purpose we consider several possibilities to obtain a measure for the size of these axially symmetric boson star solutions. We define area-type radii via introducing first the function $R(r)$,

$$R(r) = \left(\frac{1}{4\pi}\int_\Omega \sqrt{g_{\varphi\varphi}g_{\theta\theta}}|_r d\Omega\right)^{1/2}, \tag{28}$$

and then using this $R(r)$ to obtain the measures for the size

$$R_A = \frac{\int j^t R(r)\sqrt{-g}d^3r}{Q} \tag{29}$$

and

$$R_{A2}^2 = \frac{\int j^t (R(r))^2\sqrt{-g}d^3r}{Q}. \tag{30}$$

Similarly, we define circumferential-type radii via first introducing the function

$$R(r) = \frac{1}{2\pi}\int_C \sqrt{g_{\varphi\varphi}}|_{r,\theta=\pi/2}d\varphi \tag{31}$$

and then using this $R(r)$ to obtain R_C as in Eq. (29) and R_{C2}^2 as in Eq. (30). All these definitions give rather similar results. We demonstrate this (in part) in Fig. 12, where we compare the radii R_{A2}, R_A, and R_{C2}.

The figure clearly shows that the dependence of the mass on the size is very similar for rotating and nonrotating boson stars. Focusing on the smaller values of κ (away from the mini-boson star limit) the mass increases along the first branch, while the size decreases, until the cusp A is reached, marking the end of the lower density phase. Between A and B the mass decreases with decreasing size. Beyond B the mass then rises steeply again, while the size also increases along (most of) this third branch. This high density phase of the rotating boson stars then ends at the cusp C, where the spiral starts.

4. Black hole limit

As in the case of the nonrotating boson stars, we would now like to address the black hole limit for these rotating boson stars. For this purpose we employ these radii to compare the boson star masses and sizes with those of

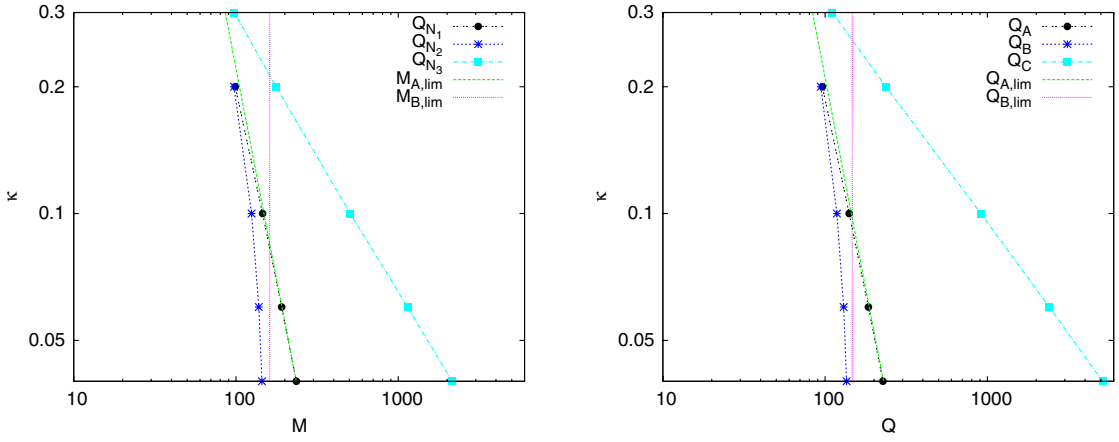

FIG. 11 (color online). Coupling constant κ versus the mass M (left panel) and versus the particle number Q (right panel) for the cusps A, B, and C, together with functions approximating the behavior of A and B in the limit $\kappa \to 0$. Note that for the larger values of κ the cusps A and B are no longer present.

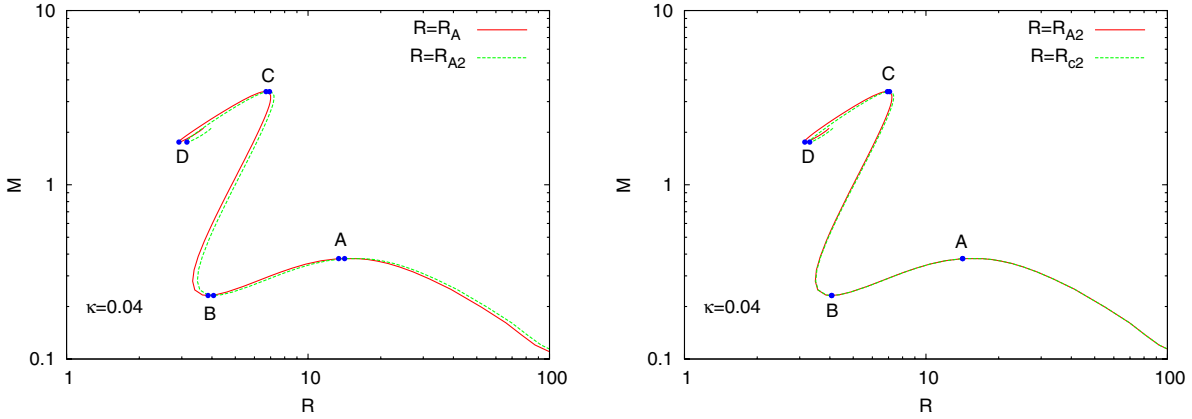

FIG. 12 (color online). A comparison of different radius definitions for $n = 1^+$ rotating boson stars: R_A and R_{A2} (left panel), and R_{A2} and R_{C2} (right panel) for $\kappa = 0.04$.

the corresponding rotating Kerr black holes. In particular, for the set of values of the size R_{A2} and angular momentum J of the boson stars, their mass M is compared with the mass $M_{\rm BH}$ of the corresponding Kerr black holes, which are evaluated for the same values of R_{A2} and J, where R_{A2} is defined via the event horizon area. We exhibit this comparison in Fig. 13 for $\kappa = 0.04$. We note that because of this construction of the Kerr curve, it has as many branches as the boson star curve. Interestingly, we observe that as in the case $n = 0$, also the rotating boson stars are very close to the black hole limit when the spiral is formed, as seen in Fig. 13 (left panel). (The spiral is enlarged in the inset, which also features the Kerr black hole branch corresponding to the steep high density boson star branch.)

For a given mass $M_{\rm BH}$, the angular momentum $J_{\rm BH}$ of a Kerr black hole cannot exceed a certain bound, the Kerr bound, $J_{\rm BH}/M_{\rm BH}^2 \leq 1$. The Kerr bound is saturated for extremal black holes. Higher angular momenta correspond to naked singularities. When considering this scaled angular momentum $J_{\rm BH}/M_{\rm BH}^2$ versus the scaled area $A_{\rm BH}/M_{\rm BH}^2$ of the black holes, all Kerr black holes fall onto a single line, starting from the point corresponding to the set of Schwarzschild solutions and ending at the point corresponding to the set of extremal Kerr solutions. The upper part of this line representing fast rotating Kerr black holes is exhibited in Fig. 13 (right panel).

In our comparison of the rotating boson stars with the Kerr black holes, we would now like to know how close the boson stars are to this Kerr bound when they are highly compact. Therefore, we also show J/M^2 versus R_{A2}/M for such a set of highly compact rotating boson stars in Fig. 13 (right panel). In particular, we have also indicated the point C of the boson star curve, where the spiral starts, and the point D, which is located inside the spiral. We note that the family of boson stars assumes at C its minimum value of J/M^2. For the case $\kappa = 0.04$, shown in the figure, $J/M^2 \approx 0.7$ at C. When κ increases, the value of J/M^2 at C increases ($\kappa = 0.06 : 0.78$, $\kappa = 0.1 : 0.86$, $\kappa = 0.2 : 0.92$, $\kappa = 0.3 : 0.94$). Thus these highly compact boson stars close to the black hole limit can rotate with angular momenta close to the Kerr bound.

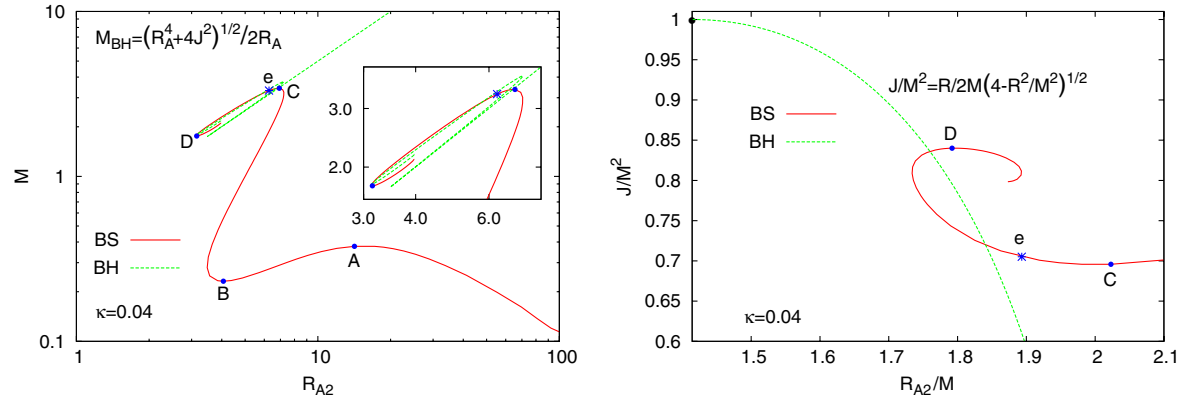

FIG. 13 (color online). Comparison of the boson star mass M versus the size R_{A2} for $\kappa = 0.04$ with the mass $M_{\rm BH}$ of the Kerr black hole obtained for the same size R and angular momentum J (left panel); comparison of the ratio J/M^2 versus the ratio R_{A2}/M of the boson stars ($\kappa = 0.04$) with the Kerr black hole curve (right panel). The point e indicates the onset of an ergoregion.

In Fig. 13 (right panel) we have also indicated the point beyond which the rotating boson stars possess ergoregions [18]. For $\kappa = 0.04$, the formation of ergoregions arises only inside the spiral. For larger values of κ the ergoregion formation starts already on the high density branch shortly before C is reached. We therefore conclude that for these $n = 1^+$ rotating boson stars, there appears to be a correlation between approaching the black hole limit and developing an ergoregion.

5. Stability analysis of $n = 1^+$ boson stars

To address the stability of these rotating boson stars, we turn to the control space $\mathcal{C} = \{\kappa, Q\}$, presented in Fig. 14. Since both $n = 0$ and $n = 1^+$ boson stars have analogous equilibrium spaces $\mathcal{M} = \{\omega_s, \kappa, Q\}$, the corresponding discussion of their stability is also analogous. From the analysis via catastrophe theory we conclude that there are two areas which possess only a single stable solution. The first area is associated with the stable branch terminating at A, formed by the stable lower density boson stars. The second area is associated with the branch from B to (almost) C, comprising the stable high density boson stars. As the coupling constant κ increases, the width of the second area diminishes and shrinks to zero at a critical value of κ. The width of the area labeled to represent two stable solutions as well as unstable solutions also diminishes with increasing κ. The width shrinks to zero at the critical value of κ, where the turning points A and B merge and disappear, while only C remains (apart from the critical points of the spiral).

According to catastrophe theory arguments the branch from the vacuum to the first turning point Q_A is a stable one. The next branch from Q_A to Q_B is unstable, while the branch from Q_B to Q_C should be stable again. The potential function for the rotating boson stars is analogous to Fig. 8. However, we must also take into account the emergence of ergoregions, which are associated with their own

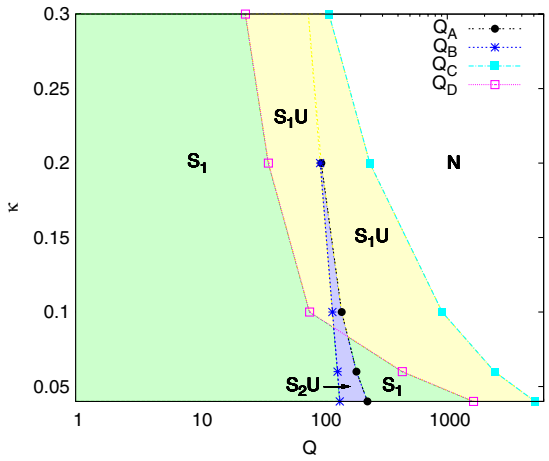

FIG. 14 (color online). Control space $\mathcal{C} = \{\kappa, Q\}$ for rotating boson stars with $n = 1^+$ in the range $0.04 \leq \kappa \leq 0.3$.

kind of instability [47–50]. While for small values of κ ergoregions arise only beyond C somewhere in the spiral, which is unstable anyway, for larger values of κ ($\kappa \geq 0.1$) ergoregions appear already along the higher density branch from B to C, signaling an instability of these highly compact rotating boson stars close to C [18,50].

Apart from this new type of instability, present only in the rotating case, the boson star solutions for the nonrotating ($n = 0$) and the rotating ($n = 1^+$) case exhibit a similar general pattern.

IV. CONCLUSIONS

We have addressed the physical properties of nonrotating and rotating boson stars, obtained with a self-interaction potential of the scalar field, which allows for nontopological soliton solutions in the absence of gravity. Such a self-interaction potential is crucial to find a much richer set of solutions than the ones obtained with only a mass term (mini-boson stars) and with a repulsive $|\Phi|^4$ interaction.

In particular, we note that there are two stable regions in the equilibrium space of the boson star solutions, when this solitonic self-interaction potential is employed, whereas there is only one such stable region for boson stars which do not possess a flat space-time limit. In fact, there is an interesting analogy to compact stars which possess a lower density phase, the white dwarf phase, and a high density phase, the neutron (or quark) star phase, since the boson stars also exhibit a lower density phase and a high density phase. Moreover, beyond the neutron star phase the compact stars exhibit an unstable spiralling phase very close to the black hole limit. Such an unstable spiralling phase very close to the black hole limit is also seen for the boson stars beyond their stable high density phase.

A stable mini-boson star is an equilibrium state, where the Heisenberg uncertainty principle $\Delta r \Delta p \sim \pi\hbar$ provides the means to balance gravity and avoid collapse below a (small) critical mass of the mini-boson stars [16]. In boson stars with a repulsive $|\Phi|^4$ potential term this self-interaction allows for much larger stable boson stars [10]. The solitonic self-interaction potential, on the other hand, has repulsive and attractive components, which dominate the features of the solutions in a large region of the equilibrium space, leaving only a minor role for gravity to play here.

Indeed, for not too large values of the coupling constant κ, the properties of the solutions follow rather closely those of the corresponding nontopological solitons. Only at the boundaries of the domain of existence, gravity becomes dominating. Here, in flat space-time, the solutions would grow without limit. Thus the single infinitely long stable branch of the nontopological solitons is reflected in the finite (mostly) stable branch $B - C$ of the boson stars. Along (most of) this branch the radius increases as the

mass increases. This branch ends when the boson star's compactness approaches the black hole limit. The soliton solutions would simply cross this limit. But as long as the coupling to gravity is finite, no matter how small it is, this limit cannot be exceeded. Thus collapse is unavoidable, as signaled by the formation of a spiral in the equilibrium space of these stationary solutions.

The single infinitely long unstable branch of the nontopological solitons, on the other hand, is reflected in the finite unstable branch $A - B$ of the boson stars. But gravity allows for an additional stable branch $0 - A$, present even in the case of no self-interaction. Here the size of the solutions decreases as the mass increases, which reveals the dominating influence of gravity for this branch.

When comparing the nonrotating ($n = 0$) and the rotating ($n = 1^+$) boson stars, we note that many of their features are very similar. While the high density soliton-type boson star branch is bounded by the Schwarzschild black holes in the $n = 0$ case, it is bounded by the Kerr black holes in the $n = 1^+$ case. Because the centrifugal force will counteract the gravitational force, it is expected that rotation stabilizes a boson star [16], and the available data indeed show that, in the presence of rotation, for given values of κ higher masses are reached for the rotating boson stars. However, rotation also comes with a *caveat* for stability, since for globally regular objects such as boson stars the presence of an ergoregion implies an instability, associated with superradiant scattering [47–50].

Thus, rotating boson stars become unstable, when they develop an ergoregion. For the $n = 1^+$ boson stars considered, the ergoregion is formed either inside the spiral or very close to the cusp C. Therefore, the possible presence of ergoregions was put forward by Cardoso *et al.* [50] as a means to scrutinize boson stars and various other black hole doubles as potential horizonless candidates for compact dark astrophysical objects. In particular, they investigated the instability time scales, showing that, depending on the mass and the angular momentum of the objects, these time scales could be rather short, such as between 0.1 sec and 1 week.

It remains to be seen whether boson stars with appropriate values of the physical parameters to fit observational data will or will not suffer from such an ergoregion instability. For the unstable ones the corresponding instability time scales will then have to be investigated. So far our analysis shows that there are stable highly compact boson stars close to the black hole limit, which are, at the same time, close to the Kerr bound $J/M^2 = 1$.

Finally, we would like to address the case of rotating boson stars with higher rotation quantum numbers $n \geq 2$. Such boson stars have been addressed by Ryan [13]. Since the numerical analysis for these systems is difficult [17,18], we have not yet accumulated a sufficient set of solutions to give a similar discussion of their properties as for the $n = 0$ and $n = 1^+$ boson stars. Still, we present in Fig. 15 a part of the equilibrium space $\mathcal{M} = \{\omega_s, \kappa, Q\}$ of the $n = 2^+$ boson stars. Whereas still higher values of the mass are reached on the soliton-type branch, we note that the onset of the ergoregion instability happens earlier, thus decreasing the viability range of these solutions.

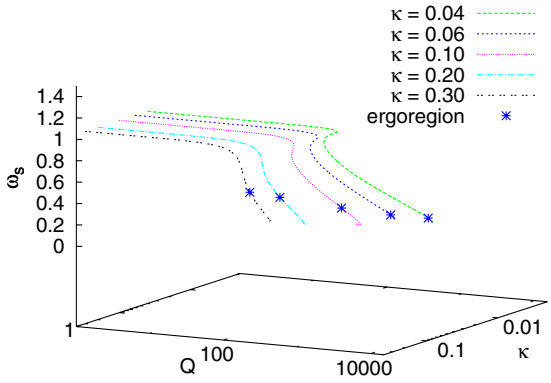

FIG. 15 (color online). Equilibrium space $\mathcal{M} = \{\omega_s, \kappa, Q\}$ for rotating boson stars with $n = 2^+$ in the range $0.04 \leq \kappa \leq 0.3$. The onset of the ergoregion is indicated by the asterisks.

Clearly, further calculations of fast rotating boson stars are called for, not only in the solitonic model but also in $|\Phi|^4$-type models, where a possible ergoregion instability has not yet been considered. Most interesting, however, will be an extension of the investigation of the dynamical evolution of boson stars [43,44,51] to the rotating case.

ACKNOWLEDGMENTS

We would like to thank Meike List and Isabell Schaffer for discussions and, in particular, for sharing their data with us. B. K. gratefully acknowledges support by the DFG.

APPENDIX A. CONSTRUCTION OF THE SOLUTIONS

1. Boundary conditions

The choice of appropriate boundary conditions must guarantee that the boson star solutions are globally regular and asymptotically flat, and that they possess finite energy and finite energy density.

For spherically symmetric boson stars boundary conditions must be specified for the metric functions $f(r)$ and $l(r)$ and the scalar field function $\phi(r)$ at the origin and at infinity. At the origin one finds the boundary conditions

$$\partial_r f|_{r=0} = 0, \qquad \partial_r l|_{r=0} = 0, \qquad \partial_r \phi|_{r=0} = 0. \quad \text{(A1)}$$

Note that for spherically symmetric boson stars the scalar field has a finite value ϕ_0 at the origin,

$$\phi(r) = \phi_0 + O(r^2). \quad \text{(A2)}$$

For $r \to \infty$ the metric approaches the Minkowski metric $\eta_{\alpha\beta}$ and the scalar field assumes its vacuum value $\Phi = 0$. Accordingly, we impose at infinity the boundary conditions

$$f|_{r\to\infty} = 1, \qquad l|_{r\to\infty} = 1, \qquad \phi|_{r\to\infty} = 0. \tag{A3}$$

For rotating axially symmetric boson stars appropriate boundary conditions must be specified for the metric functions $f(r,\theta)$, $l(r,\theta)$, $h(r,\theta)$, $\omega(r,\theta)$, and the scalar field function $\phi(r,\theta)$ at the origin, at infinity, on the positive z axis ($\theta = 0$), and, exploiting the reflection symmetry with respect to $\theta \to \pi - \theta$, in the xy plane ($\theta = \pi/2$). At the origin we require

$$\partial_r f|_{r=0} = 0, \qquad \partial_r l|_{r=0} = 0, \qquad h|_{r=0} = 1, \qquad \omega|_{r=0} = 0, \qquad \phi|_{r=0} = 0. \tag{A4}$$

At infinity the boundary conditions are

$$f|_{r\to\infty} = 1, \qquad l|_{r\to\infty} = 1, \qquad h|_{r\to\infty} = 1, \qquad \omega|_{r\to\infty} = 0, \qquad \phi|_{r\to\infty} = 0, \tag{A5}$$

and for $\theta = 0$ and $\theta = \pi/2$, respectively, we require the boundary conditions

$$\partial_\theta f|_{\theta=0} = 0, \qquad \partial_\theta l|_{\theta=0} = 0, \qquad h|_{\theta=0} = 1, \qquad \partial_\theta \omega|_{\theta=0} = 0, \qquad \phi|_{\theta=0} = 0, \tag{A6}$$

and for even parity solutions

$$\partial_\theta f|_{\theta=\pi/2} = 0, \qquad \partial_\theta l|_{\theta=\pi/2} = 0, \qquad \partial_\theta h|_{\theta=\pi/2} = 0, \qquad \partial_\theta \omega|_{\theta=\pi/2} = 0, \qquad \partial_\theta \phi|_{\theta=\pi/2} = 0, \tag{A7}$$

while for odd parity solutions $\phi|_{\theta=\pi/2} = 0$.

2. Numerical methods

First of all, because of the power law falloff of the metric functions, we compactify space by introducing the compactified radial coordinate

$$\bar{r} = \frac{r}{1+r}. \tag{A8}$$

Then the resulting set of equations is solved numerically subject to the above boundary conditions.

For spherically symmetric nonrotating solutions ($n = 0$) the set of equations depends only on the radial coordinate. It is solved numerically by employing a collocation method for boundary-value ordinary differential equations developed by Ascher, Christiansen, and Russell [52]. Here the damped Newton method of quasilinearization is applied. At each iteration step a linearized problem is solved by using a spline collocation at Gaussian points.

Rotating solutions are obtained when $n \neq 0$. The resulting set of coupled nonlinear partial differential equations is solved numerically by employing a finite difference solver [53], based on the Newton-Raphson method. The equations are discretized on a nonequidistant grid in $\bar{r}$ and θ. Typical grids used have sizes 90×70, covering the integration region $0 \leq \bar{r} \leq 1$ and $0 \leq \theta \leq \pi/2$.

[1] S. L. Shapiro and S. A. Teukolsky, *Black Holes, White Dwarfs, and Neutron Stars: The Physics of Compact Objects* (Wiley, New York, USA, 1983).
[2] D. A. Feinblum and W. A. McKinley, Phys. Rev. **168**, 1445 (1968).
[3] D. J. Kaup, Phys. Rev. **172**, 1331 (1968).
[4] R. Ruffini and S. Bonazzola, Phys. Rev. **187**, 1767 (1969).
[5] T. D. Lee and Y. Pang, Phys. Rep. **221**, 251 (1992).
[6] P. Jetzer, Phys. Rep. **220**, 163 (1992).
[7] A. R. Liddle and M. S. Madsen, Int. J. Mod. Phys. D **1**, 101 (1992).
[8] E. W. Mielke and F. E. Schunck, *Proceedings of the 8th Marcel Grossmann Meeting in Jerusalem* (World Scientific, Singapore, 1999), p. 1607.
[9] F. E. Schunck and E. W. Mielke, Classical Quantum Gravity **20**, R301 (2003).
[10] M. Colpi, S. L. Shapiro, and I. Wasserman, Phys. Rev. Lett. **57**, 2485 (1986).
[11] R. Friedberg, T. D. Lee, and Y. Pang, Phys. Rev. D **35**, 3658 (1987).
[12] F. E. Schunck and E. W. Mielke, Phys. Lett. A **249**, 389 (1998).
[13] F. D. Ryan, Phys. Rev. D **55**, 6081 (1997).
[14] S. Yoshida and Y. Eriguchi, Phys. Rev. D **56**, 762 (1997).
[15] F. E. Schunck and E. W. Mielke, Gen. Relativ. Gravit. **31**, 787 (1999).
[16] E. W. Mielke and F. E. Schunck, Nucl. Phys. **B564**, 185 (2000).
[17] B. Kleihaus, J. Kunz, and M. List, Phys. Rev. D **72**, 064002 (2005).
[18] B. Kleihaus, J. Kunz, M. List, and I. Schaffer, Phys. Rev. D **77**, 064025 (2008).
[19] Y. Brihaye and B. Hartmann, Nonlinearity **21**, 1937 (2008).
[20] Y. Brihaye and B. Hartmann, Phys. Rev. D **79**, 064013 (2009).
[21] Y. Brihaye, T. Caebergs, B. Hartmann, and M. Minkov, Phys. Rev. D **80**, 064014 (2009).
[22] D. Astefanesei and E. Radu, Nucl. Phys. **B665**, 594 (2003).
[23] T. D. Lee and Y. Pang, Nucl. Phys. **B315**, 477 (1989).

[24] F. V. Kusmartsev, E. W. Mielke, and F. E. Schunck, Phys. Rev. D **43**, 3895 (1991).
[25] F. V. Kusmartsev and F. E. Schunck, Physica B (Amsterdam) **178**, 24 (1992).
[26] R. Thom, *Structural Stability and Morphogenesis* (W. A. Benjamin, Reading, MA, 1976).
[27] E. C. Zeeman, *Catastrophe Theory* (Addison-Wesley, Reading, MA, 1977).
[28] T. Poston and I. Stewart, *Catastrophe Theory and its Applications* (Pitman, New York, 1978).
[29] I. Stewart, Physica D (Amsterdam) **2** 245 (1981).
[30] V. I. Arnol'd, S. M. Gusein-Zade, and A. N. Varchenko, *Singularities of Differential Maps* (Birkhäuser, Boston, 1985), Vol. I.
[31] V. I. Arnol'd, *Catastrophe Theory* (Springer-Verlag, Berlin and Heidelberg, 1992).
[32] F. V. Kusmartsev, Phys. Rep. **183**, 1 (1989).
[33] M. S. Volkov and E. Wöhnert, Phys. Rev. D **66**, 085003 (2002).
[34] T. Tamaki and N. Sakai, Phys. Rev. D **81**, 124041 (2010).
[35] T. Tamaki and N. Sakai, Phys. Rev. D **83**, 044027 (2011).
[36] B. Kleihaus and J. Kunz, Phys. Rev. D **57**, 834 (1998).
[37] B. Kleihaus and J. Kunz, Phys. Rev. D **57**, 6138 (1998).
[38] B. Kleihaus and J. Kunz, Phys. Rev. Lett. **86**, 3704 (2001).
[39] B. Kleihaus, J. Kunz, and F. Navarro-Lerida, Phys. Rev. D **66**, 104001 (2002).
[40] R. M. Wald, *General Relativity* (University of Chicago Press, Chicago, 1984).
[41] E. Witten, Phys. Rev. D **30**, 272 (1984).
[42] E. Farhi and R. L. Jaffe, Phys. Rev. D **30**, 2379 (1984).
[43] E. Seidel and W.-M. Suen, Phys. Rev. D **42**, 384 (1990).
[44] J. Balakrishna, E. Seidel, and W.-M. Suen, Phys. Rev. D **58**, 104004 (1998).
[45] H. Whitney, Ann. Math. **62**, 374 (1955).
[46] B. Hartmann, B. Kleihaus, J. Kunz, and M. List, Phys. Rev. D **82**, 084022 (2010).
[47] J. L. Friedman, Commun. Math. Phys. **63**, 243 (1978).
[48] N. Comins and B. F. Schutz, Proc. R. Soc. A **364**, 211 (1978).
[49] S. Yoshida and Y. Eriguchi, Mon. Not. R. Astron. Soc. **282**, 580 (1996).
[50] V. Cardoso, P. Pani, M. Cadoni, and M. Cavaglia, Phys. Rev. D **77**, 124044 (2008).
[51] F. S. Guzman, Rev. Mex. Fis. **55**, 321 (2009).
[52] U. Ascher, J. Christiansen, and R. D. Russell, Math. Comput. **33**, 659 (1979); U. Ascher, J. Christiansen, and R. D. Russell, ACM Trans. Math. Softw. **7**, 209 (1981).
[53] W. Schönauer and R. Weiß, J. Comput. Appl. Math. **27**, 279 (1989); M. Schauder, R. Weiß, and W. Schönauer, The CADSOL Program Package, Universität Karlsruhe, Interner Bericht No. 46/92, 1992.